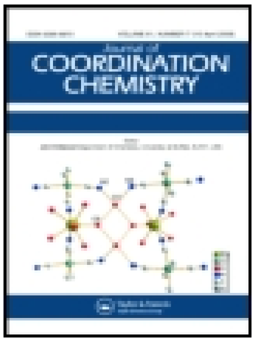

Taylor & Francis
Taylor & Francis Group

Journal of Coordination Chemistry

ISSN: 0095-8972 (Print) 1029-0389 (Online) Journal homepage: http://www.tandfonline.com/loi/gcoo20

Ring-expanded iridium and rhodium N-heterocyclic carbene complexes: a comparative DFT study of heterocycle ring size and metal center diversity

E. Ö. Karaca, M. Akkoç, E. Öz, S. Altin, V. Dorcet, T. Roisnel, N. Gürbüz, Ö. Çelik, A. Bayri, C. Bruneau, S. Yaşar & I. Özdemir

To cite this article: E. Ö. Karaca, M. Akkoç, E. Öz, S. Altin, V. Dorcet, T. Roisnel, N. Gürbüz, Ö. Çelik, A. Bayri, C. Bruneau, S. Yaşar & I. Özdemir (2017): Ring-expanded iridium and rhodium N-heterocyclic carbene complexes: a comparative DFT study of heterocycle ring size and metal center diversity, Journal of Coordination Chemistry, DOI: 10.1080/00958972.2017.1287906

To link to this article: http://dx.doi.org/10.1080/00958972.2017.1287906

JOURNAL OF COORDINATION CHEMISTRY, 2017
http://dx.doi.org/10.1080/00958972.2017.1287906

Taylor & Francis
Taylor & Francis Group

Ring-expanded iridium and rhodium *N*-heterocyclic carbene complexes: a comparative DFT study of heterocycle ring size and metal center diversity

E. Ö. Karaca[a], M. Akkoç[a], E. Öz[b], S. Altin[b], V. Dorcet[c], T. Roisnel[c], N. Gürbüz[a], Ö. Çelik[d], A. Bayri[b], C. Bruneau[c], S. Yaşar[a] and I. Özdemir[a]

[a]Department of Chemistry, İnönü University, Malatya, Turkey; [b]Department of Physics, İnönü University, Malatya, Turkey; [c]Université de Rennes, UMR 6226: CNRS Sciences Chimiques de Rennes, Rennes, France; [d]Department of Physics, Dicle University, Diyarbakır, Turkey

ABSTRACT

A new series of ring-expanded six- and seven-membered *N*-heterocyclic carbene precursors (re-NHCs) and their transition metal complexes were synthesized. The basic properties of the synthesized materials were investigated by density functional theory (DFT). The six- and seven-membered re-NHCs were synthesized in good yield via reaction of the corresponding alkyldibromides or alkyldiiodides with *N*,*N′*-bis-(2-phenylbenzene)formamidine in the presence of K_2CO_3 under aerobic conditions. Complexes, represented by the formula [$ML_{1,2}$(COD)Cl] (where M = Ir or Rh and L is a ring-expanded *N*-heterocyclic carbene ligand), were synthesized in the presence of the corresponding free carbene and iridium or rhodium metal precursors in tetrahydrofuran. All new re-NHC complexes were characterized by different analytical techniques, including NMR spectroscopy, X-ray diffraction, UV spectroscopy and elemental analysis. According to molecular electrostatic potential calculations, the electrophilic properties of the complexes were aligned, from highest to lowest, as Ir-6-DiPh, Rh-6-DiPh and Ir-7-DiPh. The HOMO, LUMO and energy gaps of the complexes were calculated by DFT. On the basis of the DFT analysis, it can be predicted that Rh-6-DiPh is the most stable complex and Ir-7-DiPh is more reactive than Ir-6-DiPh.

ARTICLE HISTORY
Received 11 September 2016
Accepted 29 December 2016

KEYWORDS
Iridium; rhodium; *N*-Heterocyclic carbene; DFT calculation; X-ray

CONTACT S. Yaşar syasar44@gmail.com, sedat.yasar@inonu.edu.tr

Supplemental data for this article can be accessed http://doi.dx.org/10.1080/00958972.2017.1287906.

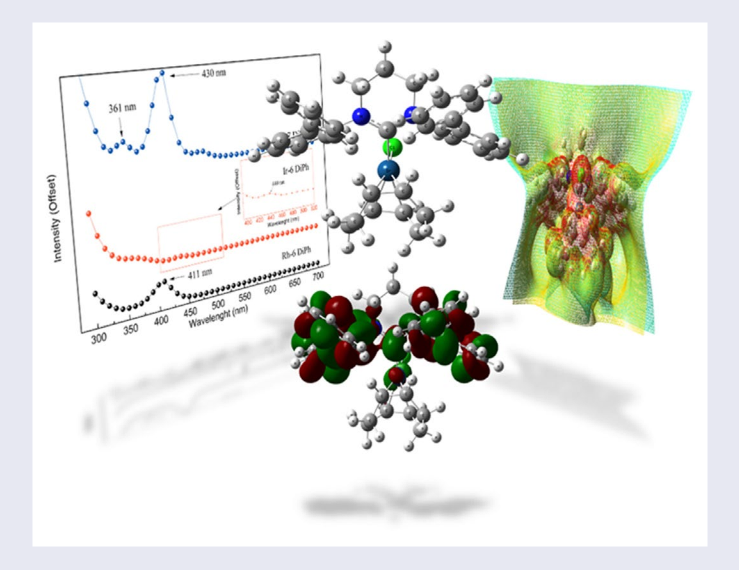

1. Introduction

Ligands are extremely important for metal complexes. *N*-heterocyclic carbenes (NHCs) are among the most important ligands in organometallic chemistry and catalysis in the last few decades due to their unique tunable steric and electronic parameters and strong metal-carbon bonds [1]. It is well known that NHCs can be easily tuned by changing the groups on the nitrogen atom and the ring size [2]. Until now, the majority of studies have focused on imidazole-, imidazolidine- and benzimidazole-based NHCs. Insufficiently explored expanded-ring NHCs (re-NHCs) have drawn much attention recently because they offer significantly different steric and electronic properties. The expanded ring on NHCs leads to a significant increase in the donor ability and steric hindrance to the metal center. Therefore, the unique tunable steric and strong σ-donation properties of expanded-ring NHCs make them desirable ligands for transition metals [1–3].

The preliminary work on re-NHCs was carried out by the groups of Stahl and Cavell. They reported the synthesis and catalytic application of six-, seven- and eight-membered NHCs and their Pd, Ir, Rh, Ag and Au complexes [1, 3c, 3d, 4]. According to their findings, large rings and N-C_{NHC}–N bond angles offer steric and electronic advantages compared to conventional five-membered analog derivatives in catalytic applications. The key points of these ligands are the basic carbon and the steric effect on the metal center [5]. As a result of these features, Re-NHCs have demonstrated unique activity in C–C coupling [3c], hydrosilylation [6], hydrogenation [7] and transfer hydrogenation [8].

To better understand the nature and behavior of this class of ligands, herein we report the synthesis and characterization of the more sterically demanding 6-DiPh.HBr- and 7-DiPh.HBr-membered NHC precursors, which bear a diphenyl group, and their iridium(I) and rhodium(I) complexes. Density Functional Theory (DFT) calculations of their properties are also presented.

2. Results and discussion

As seen in Figure 1, 6-DiPh.HBr and 7-DiPh.HI were synthesized in good yields (80–90%) by known methods starting from commercially available reagents [3a, 3c, 4, 6]. The

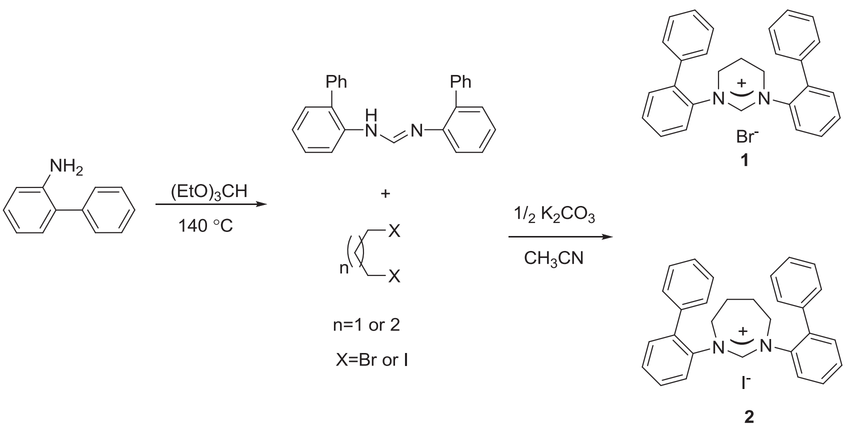

Figure 1. Synthesis of **1** (6-DiPh.HBr) and **2** (7-DiPh.HI) ring expanded N-heterocyclic carbene precursors.

nonhygroscopic re-NHC precursors (Figure 1) were fully characterized by ^{1}H and ^{13}C NMR and LCMS-MS spectroscopies. The ^{1}H NMR spectra of the re-NHC salts supported the assigned structures and the resonances for acidic C(2)–H were observed as sharp singlet signals at 7.77 and 8.56 ppm for **1** and **2**, respectively. The ^{13}C NMR chemical shifts were consistent with the proposed structure and the imino carbon appeared as a typical singlet in the ^{1}H-decoupled mode at 154.7 and 160.3 ppm for **1** and **2**, respectively.

The ring-expanded iridium(I) and rhodium(I)-carbene complexes **3–5** with the general formula [M(NHC)(COD)Cl] were obtained through direct addition of *in situ* generated free carbene to the corresponding dimeric $[IrCl(COD)]_2$ and $[RhCl(COD)]_2$ precursors in tetrahydrofuran (THF) under inert conditions. This afforded the desired complexes **3–5** as air stable yellow or orange solids in yields ranging from 40 to 80% (Figure 2) [5a, 9, 10]. Synthesis of the iridium and rhodium complexes was attempted using a transmetalation method from silver(I) to iridium and rhodium metals. Unfortunately, we could not obtain any isolated rhodium or iridium complexes from *in situ* transmetalation from silver(I).

Our observation contrasts with that of Nechaev [4a], but consistent with the observations of Herrmann [11], Cavell [4c, 4d, 5a] and Buchmeiser [12, 13]. According to Nechaev, transmetalation is reversible with bulky six- and seven-membered NHCs [4a]. This approach seems to be compatible with our results.

The ^{13}C{^{1}H} NMR shift of the carbenic carbons of **3–5** were observed at 205.9, 212.3 and 216.7 ppm, respectively, and a downfield shift in resonance with increasing heterocycle-ring size was observed. This result is consistent with previous observations [11–13].

Complex **3** was investigated by X-ray crystal structure analysis. A single crystal suitable for X-ray diffraction (XRD) was obtained by slow vapor diffusion of diethylether into a concentrated dichloromethane solution of the complex in question [14]. Single crystal XRD was carried out at 293(2) K using a Bruker APEX-II CCD diffractometer. The intensity data were collected using graphite monochromated MoKα ($\lambda = 0.71073$ Å) radiation. The structure was solved by direct method SHELXS-97 software [14] and refined by full-matrix least-squares on F^2 using SHELXL-97 with refinement of F^2 against all reflections. Reflections collected/uniquely used 7000/4557 [$R_{int} = 0.022$]/4557, 181 parameters refined, $[\Delta\rho]_{max}/[\Delta\rho]_{min} = 3.691/-2.931$ eÅ^{-1}, $R1/wR2$ (for all data) = 0.054/0.081. Hydrogen atoms were constrained by difference maps and refined isotropically. Other atoms were refined anisotropically. For absorption

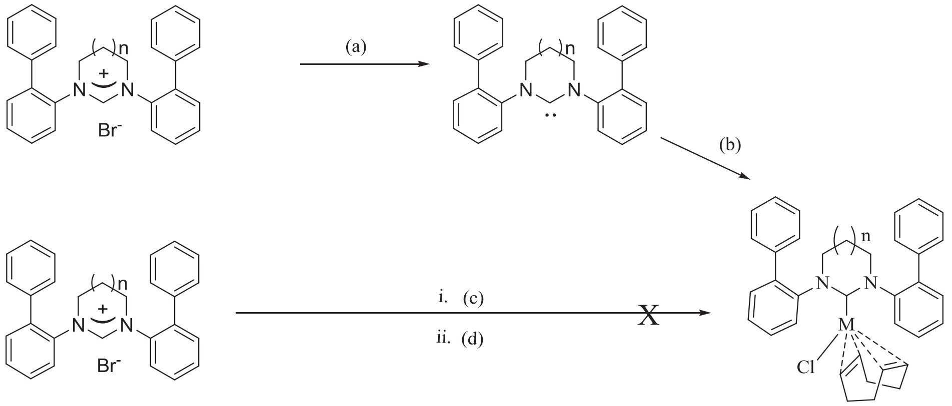

(a) KHMDS, THF, r.t.; (b) $[MCl(COD)]_2$, THF, r.t.
(c) Ag_2O, DCM, r.t.; (d) $[MCl(COD)]_2$, DCM, r.t.

n=1,M=Ir, 3
n=1,M=Rh, 4
n=2,M=Ir, 5

Figure 2. Preparation of iridium and rhodium Re-NHC complexes.

correction, a multi-scan Bruker (2005), SADABS Bruker AXS Inc., Madison, Wisconsin, USA was applied. The molecular structure plots were prepared using PLATON and ORTEPIII [15]. The crystal data, experimental parameters, anisotropic thermal parameters, structure factors (observed and calculated) and a full list of bond distances, bond angles and torsion angles are given in the Supplementary Material.

A perspective view of the molecular structure of **3–5** with the atom numbering scheme is given in Figure 3. The bond lengths (Å) and angles (°) for **3** are given in Table 1. The Ir atom lies on a crystallographic center of symmetry and is coordinated to five C and Cl atoms. The Ir–C and Ir–Cl average bond lengths are 2.103(3) Å and 2.3989(17) Å, respectively. These values are in agreement with the literature [16, 17]. As expected, **3–5** have a distorted square-planar geometry. Each iridium and rhodium center were coordinated to a re-*N*-heterocyclic carbene ligand, a chloro atom and η^4-coordinated 15-cyclooctadiene (COD), giving rise to four-coordinate environments. The dihedral angles between P1-P2, P1-P3 and P2-P3 (P1:(Ir/C1/C2/C3/C4), P2:(C8/C9/C10/C11/C12/C13) and P3:(C14/C15/C16/C17/C18/C19)) are 38.25°, 89.95° and 53.16°, respectively. Pyrimidine rings are in a *cis*-configuration. The C5/N1/C6/C7/C6–1/N1–1 ring has a boat-like configuration [18]. The torsion angles of C9–C8–N1–C5and C9–C8–N1–C6 are 63.1° and 108.6°, respectively. A summary of the crystallographic data for **3** is provided in Table 1. For **4** and **5**, see supplementary file. In addition, the structures of **3–5** were investigated by DFT calculations. It can be seen in Table 2a–c that the experimental data and theoretical calculations are in agreement for **3–5**. The numerical estimation of crystallographic data is in accord with experimental results.

The hydrogen bond molecular geometry values and hydrogen-bonding geometries between some atoms and C for the ring center of gravity (Å) for **3** are given in Table 3. The molecular geometry was affected by the two C–H … Cl and C–H … N intramolecular hydrogen-bond interactions. Otherwise, there are two C–H … Cg interactions between the atom and the ring center of gravity. The ring center of gravities are Cg(1):C8/C9/C10/C11/C12/C13 and Cg(2):C14/C15/C16/C17/C18/C19.

With different symmetry codes, such as –x,–y,1-z, –x,–y,1-z and 1-x,–y,1-z, Cg(1) and Cg(2), given in Table 4, *π*–*π* interactions and their view without H atoms are given in Figure 4. The

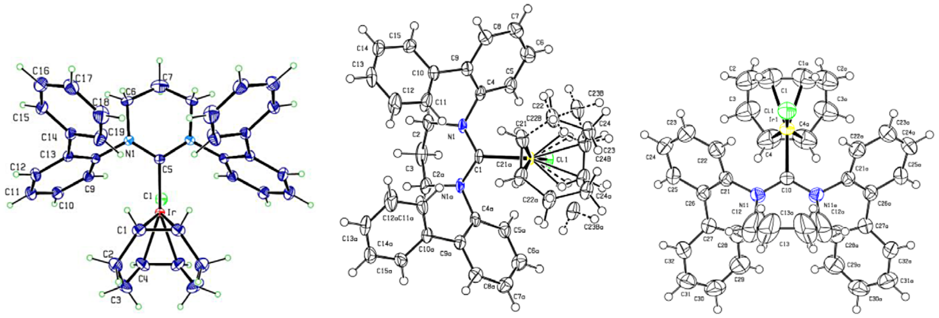

Figure 3. ORTEP ellipsoid plot at 50% probability of the molecular structure of **3**, **4** and **5**, respectively. Hydrogens have been omitted for clarity.

Table 1. Selected bond lengths (Å), angles (°) and torsion angles (°) of 3.

Bond	Distance (Å)	Torsion angle	(°)
Ir–C5	2.054(3)	C5–Ir–C4–C3	−75.9(8)
Ir–C1	2.094(3)	C1–Ir–C4–C3	3.5(5)
Ir–C4	2.162(4)	Cl–Ir–C4–C3	−159.3(5)
Ir–Cl	2.3989(17)	C8–N1–C5–Ir	4.5(4)
N1–C5	1.351(3)	C6–N1–C5–Ir	−166.4(3)
N1–C8	1.439(3)	C4–Ir–C5–N1	−5.8(7)^{ii}
N1–C6	1.475(4)	C1–Ir–C5–N1	−71.5(3)
Bond angle	(°)	C4–Ir–C5–N1	5.8(7)
C5–Ir–C1	94.96(14)	Cl–Ir–C5–N1	88.8(3)
C5–Ir–C4	161.69(15)	C3–C2–C1–Ir	22.9(7)
C1–Ir–C4	81.32(19)	C5–Ir–C1–C2	148.3(3)^{ii}
C5–Ir–Cl	90.31(10)	C1–Ir–C1–C2	−120.0(3)^{ii}
C1–Ir–Cl	159.59(12)	C4–Ir–C1–C2	−13.7(3)
C4–Ir–Cl	87.50(17)	Cl–Ir–C1–C2	43.9(5)
C3–C4–Ir	114.5(4)	Ir–C4–C3–C2	8.0(8)
C2–C1–Ir	111.2(4)	C5–N1–C6–C7	18.9(7)

package view of **3** (without H atoms and along the *a*-axis) is also given (Supplementary Material, figure S1).

2.1. Computational methods

DFT computations of **3–5** were performed using the GAUSSIAN 09 W software package [19] with the B3LYP (Becke, 3-parameter, Lee-Yang-Parr)/LanL2DZ (Los Alamos National Laboratory 2 Double Zeta) basis set.

Firstly, the geometries of the complex structures were optimized to obtain the global minimum energy geometries. Afterward, UV–vis calculations performed with the same basis set were used for the optimized molecule structures. The energy of the excited states together with the ground-states for the optimized molecules were computed using DFT and visualized by the GAUSSVIEW 5 software package [20].

2.2. Molecular electrostatic potential

Molecular electrostatic potential (MEP) analysis is a technique that shows the mapping of the electrostatic potential surface of a complex using constant electron density which can

Table 2a. Analogy of experimental and theoretical computation bond length and angle results of **3**.

	Ir-6–DiPh	Ir-6–DiPh
	(Exp.)	(DFT)
Bond	Length (Å)	Length (Å)
Ir–C5	2.054(3)	2.07818
Ir–C1	2.094(3)	2.15006
Ir–C1 *	2.094(3)[ii]	2.13750
Ir–C4	2.162(4)	2.22762
Ir–C4 *	2.162(4)[ii]	2.25420
Ir-–Cl	2.3989(17)	2.56906
N1–C5	1.351(3)	1.37799
N1–C8	1.439(3)	1.45534
N1–C6	1.475(4)	1.49925
Angle	(°)	(°)
C5–Ir–C1	94.96(14)	96.171
C5–Ir–C1 *	94.96(14)[ii]	93.35947
C1–Ir–C1	39.3(2)[ii]	39.5402
C5–Ir–C4	161.69(15)	159.72787
C1–Ir–C4	81.32(19)	80.60365
C1–Ir–C4 *	93.38(19)[ii]	88.29325
C5–Ir–C4	161.69(15)[ii]	159.72787
C1–Ir–C4	93.38(19)[ii]	88.29325
C1–Ir–C4	81.32(19)[ii]	80.60365
C4–Ir–C4	36.3(3)[ii]	36.84753
C5–Ir-–Cl	90.31(10)	90.43165
C1–Ir-–Cl	159.59(12)	161.47182
C1–Ir–Cl *	159.59(12)[ii]	157.44696
C4–Ir–Cl	87.50(17)	87.20786
C4–Ir–Cl *	87.50(17)[ii]	89.85563
C4–C4–Ir	71.83(15)[ii]	70.55637
C3–C4–Ir	114.5(4)	109.61261
N1–C5–Ir	122.09(15)[ii]	122.09478
N1–C5–Ir	122.09(15)[ii]	121.88927
C1–C1–Ir	70.34(12)	70.69689
C2–C1–Ir	111.2(4)	114.83943

be obtained using the molecular size, shape and electrostatic potential value. The electrostatic potential of compounds is due to the potential related to dipole moments, electronegativity, partial charges and the site of chemical reactivity of the molecule [21]. The positive electrostatic potential corresponds to repulsion of the protons by the nuclei and the negative electrostatic potential is due to the attraction of electrons by nuclei [21]. Furthermore, the electrostatic potential around the molecule can be defined as the energy between the charge distribution of the molecule and a unit positive test charge, as shown below:

$$V(r) = \sum_{A} \frac{Z_A}{|R_A - r|} - \int \frac{\rho(r^1)}{|r^1 - r|}\,\mathrm{d}r^1$$

where Z_A is the charge of nucleus A in RA, $\rho(r^1)$ is the density of the charge at r^1 and r^2 is the dummy integration variable [22, 23]. The MEP of the complexes can also give information about electrophilic and nucleophilic attack in the molecules. The MEP results for the complexes are given (figure S2a–c). While the green bump regions on the complexes correspond to positive electrostatic region, the red sink regions represent the negative electrostatic potential regions (figure S2a–c) for **3–5**. The value of the positive charged region is low when compared with the negative charged region (figure S2a–c). Thus, it can be predicted that the complexes have nucleophilic character and are sensitive against electrophilic attack. It

Table 2b. Analogy of experimental and theoretical computation bond length and angle results of **4**.

	Rh-6–DiPh	Rh-6–DiPh
	(Exp.)	(DFT)
Bond	Length (Å)	Length (Å)
Rh–C1	2.061	2.08086
Rh–C21	2.119	2.17221
Rh–C21a	2.119	2.15428
Rh–C24	2.192	2.27365
Rh–C24a	2.192	2.30597
Rh–C24b	2.192	2.20583
N–C10	1.342	1.37387
N–C21	1.444	1.45551
N–C12	1.481	1.50042
Angle	(°)	(°)
C1–Rh–C21	94.1	96.55341
C1–Rh–C21a	94.1	93.19030
C21–Rh–C21a	39.8	38.60115
C1–Rh–C24	162.01	160.93880
C21Rh C24b	81.6	80.66932
C21–Rh–C24b	93.6	87.90624
C1–Rh–C24	162.01	160.93880
C21–Rh–C24	81.6	80.66932
C21–Rh–C24	93.6	80.39730
C24–Rh–C24	35.8	35.50085
C1–Rh–Cl	90.44	90.35779
C21–Rh–Cl	159.54	162.46872
C21–RhCl	159.54	157.27202
C24–Rh–Cl	88.04	87.53717
C24b–Rh–Cl	88.04	89.98380
C24–C24–Rh	72.8	70.98638
C22–C21–Rh	106.3	107.42468
N1–C1–Rh	121.6	121.70071
N1a–C1–Rh	121.6	121.69516
C24–C24–Rh	72.08	71.37705
C23b–C22b–Rh	115.6	113.84766

is seen that the electrophilic region of the complexes have small values, meaning a weak attractive potential for negative complexes, but the red region has a good electrophilic effect, especially in the region of Cl ions. From the time dependent DFT calculations, the electrophilic properties of the complexes align from highest to lowest as **3**, **4** and **5** by the intensity of the red region.

2.3. HOMO and LUMO analysis

The B3LYP/LanL2DZ basis set was used for the calculation of the energy of the highest occupied molecular orbital (HOMO) and the lowest unoccupied molecular orbital (LUMO). The HOMO and LUMO orbitals of **3–5** are given in Figure 5. It is well known that the HOMO and LUMO orbitals and the energy gap, which can be calculated from the energy of the HOMO and LUMO, are correlated for the chemical activity of molecules.

While the HOMO acts as an electron donor to donate an electron, the LUMO acts as an acceptor to accept an electron. The obtained values from DFT are given in Table 5. The highest HOMO and LUMO energies are obtained for **5** and the lowest HOMO and LUMO energies are observed for **4**. Therefore, when the energy gaps of the complexes are ranked in order from highest to lowest, they can be written as **4**, **3** and **5**.

Table 2c. Analogy of experimental and theoretical computation bond length and angle results of **5**.

	Ir-7–DiPh	Ir-7–DiPh
	(Exp.)	(DFT)
Bond	Length (Å)	Length (Å)
Ir–C10	2.053	2.05877
Ir–C4	2.111	2.15105
Ir–C4*	2.111	2.13775
Ir–C1	2.164	2.23902
Ir–C1*	2.164	2.27080
Ir–Cl	2.407	2.56484
N–C10	1.353	1.37688
N–C21	1.449	1.45926
N–C12	1.481	1.50508
Angle	(°)	(°)
C10–Ir–C4	95.8	98.47423
C10–Ir–C4a	95.8	94.88054
C4–Ir–C4*	38.8	39.53973
C10–Ir–C1	161.7	160.07156
C4–Ir–C1	81.1	80.31240
C1–Ir–C4	89.06	88.42896
C10–Ir–C1	161.7	162.92951
C4–Ir–C1a	93.04	88.42896
C4–Ir–C1	93.0	96.48108
C4–Ir–C4	38.2	36.53316
C10–Ir–Cl	89.06	88.45510
C4–Ir–Cl	160.0	162.63069
C4a–Ir–Cl	160.0	156.14242
C1–Ir–Cl	88.2	87.74727
C1a–Ir–Cl	88.2	89.42668
C1–C1–Ir	71.9	70.51058
C2–C1–Ir	109.5	109.46238
N11–C10–Ir	121.2	121.60599
N11a–C10–Ir	121.2	123.37961
C4–C4–Ir	70.6	70.72443
C3–C4–Ir	112.8	115.08804

Table 3. Hydrogen-bond interactions for **3**.

D–H … Cg	D–H (Å)	H … Cg (Å)	D … Cg (Å)	D–H … Cg (°)
C4–H4 ... Cl	0.980(5)	2.955(2)	3.159(7)	92.83(35)
C9–H9 ... Cl	0.930(3)	2.552(1)	3.356(3)	144.90(19)
C19–H19 ... N1	0.930(4)	2.884(3)	3.183(5)	100.17(30)
C12–H12 … Cg2^{ii}	0.930(4)	3.044(2)	3.681(5)	127.19(14)
C15–H15 … Cg1^{iii}	0.930(5)	3.098(2)	3.768(5)	130.38 (18)

Cg1:C8/C9/C10/C11/C12/C13, Cg(2):C14/C15/C16/C17/C18/C19.
Symmetry codes: [ii] 1−x,−y,1−z; [iii] −x,−y,1−z.

Table 4. π–π Interactions for **3**.

Cg–Cg	Cg–Cg (Å)	Dihedral angle (°)	Symmetry code
Cg(1)–Cg(1)	5.225(4)	26.69	−x,−y,1−z
Cg(1)–Cg(2)	4.907(4)	24.52	−x,−y,1−z
Cg(2)–Cg(1)	4.797(4)	64.11	1−x,−y,1−z

From the DFT calculations, it can be predicted that **4** is the most stable complex and that **5** is more reactive than **3**. This observation is consistent with the work of Whittlesey and Cavell [24]. They carried out a comparative study of ring-expanded NHCs with the focus on

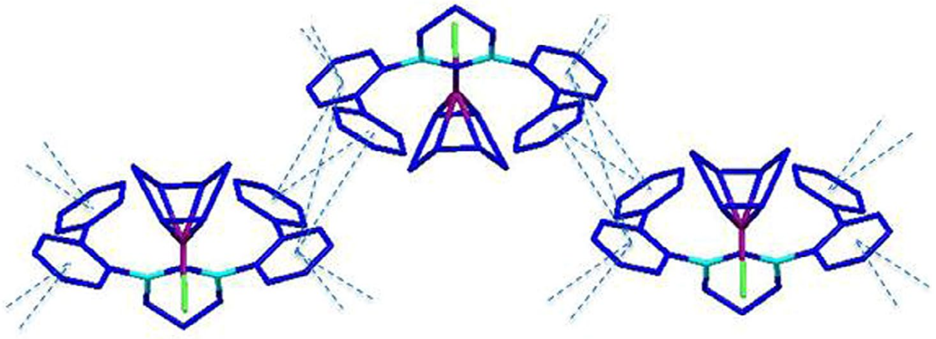

Figure 4. π–π Interactions for **3** (without H atoms) obtained by single crystal X-ray diffraction of experimentally obtained crystal.

ring size in transition metal-catalyzed reactions. An upward trend in activity of the re-NHC complexes was observed with increasing heterocycle ring size [24].

2.4. Photophysical properties of 3–5

The molecular orbitals of the complexes are related to the electronic transition process that has strong correlation photophysical properties, such as UV–vis spectra, which are shown in Table 6. Also, theoretical and experimental UV–vis spectra of complexes are compared in Table 6; the results were found to be compatible.

The complexes in this study have a transition metal in a distorted square-planar environment, as given in the structural properties section. The fivefold degenerate d-orbitals on a transition metal in the pure square-planar environment (D_{4h}) generally split to four different level orderings of b_{1g} ($x^2 - y^2$) > b_{2g} (xy) > e_g (xz,yz) > a_{1g} (z^2) and the splitting energy for different coordination of d-orbitals can be in a range of visible color regions. The colors of the square planar complexes are due to some d–d transitions together with charge transfer from either the ligand-to-metal or metal-to-ligand [25].

It is already quite well known that for square-planar complexes there are three spin-allowed d–d transitions corresponding to $^1A_{1g}$–$^1A_{2g}$, $^1A_{1g}$–^1E_g and $^1A_{1g}$–$^1B_{1g}$. Since parity is important for the O_h and D_{4h} systems, these three transitions are parity forbidden for electric dipole transitions, the bands of the UV–vis spectra of d-d transitions would be expected to have lower intensities. The UV–vis spectra of **3–5** are presented in Figure 6. It is seen that the bands due to d–d transitions which correspond to a pure square geometry are not detected properly. This is probably due to the distortion from the square-planar geometry on the complexes. In this case, the energy of d electrons would be different from the pure square-planar environments. So the molecular orbital diagram of the complexes cannot be as pictured as shown in figure S3, which is for the pure square-planar geometry. It can be noted that ordering of d electrons may change in the complexes due to level of the distortion. Hence, the term symbols mentioned in figure S3 would be different than the labeled ones for the square-planar geometry.

The extinction coefficient (ε) of each complex was calculated according to Lambert–Beer law. The calculated values of ε for complexes inserted in the UV–vis spectra, which is shown in Figure 6. It was mentioned that the bands in the UV–vis spectra of the complexes have

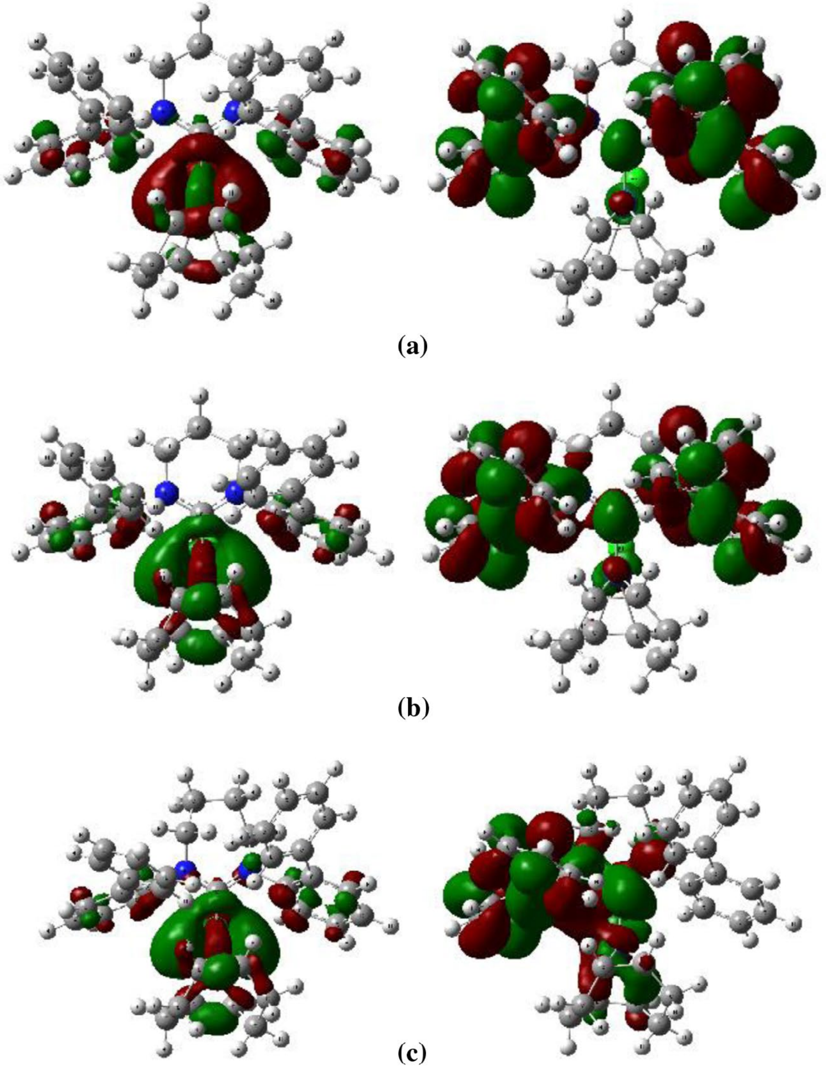

Figure 5. HOMO (left) and LUMO (right) of (a) **4**, (b) **3** and (c) **5** by DFT calculation.

Table 5. HOMO, LUMO and E_g of the complexes.

Complex	HOMO (eV)	LUMO (eV)	Eg (eV)
4	−5.1614	−1.2590	3.9024
3	−5.1160	−1.2694	3.8466
5	−5.0958	−1.4524	3.6364

more intense than the complex which has pure square-planar environment since the parity forbidden transitions would disappear. In the UV–vis spectra of **3**, the first band of highly intense absorption at around 300 nm ($\varepsilon \approx 2692\ M^{-1}\ cm^{-1}$) is mainly due to spin-allowed transitions since this shows high peak intensities in UV spectra. The band at around 360 nm ($\varepsilon \approx 7092\ M^{-1}\ cm^{-1}$) is due to ligand-metal charge-transfer transitions, and it is well known

Table 6. Comparison of calculated and experimentally obtained UV–vis results of the complexes.

Excitation wavelength (nm)					
3		5		4	
Exp.	Calc.	Exp.	Calc.	Exp.	Calc.
364	352.32	–	359.42	–	358.46
–	388.5	–	387.62	408	388.76
–	410.63	440	451.46	–	440.69

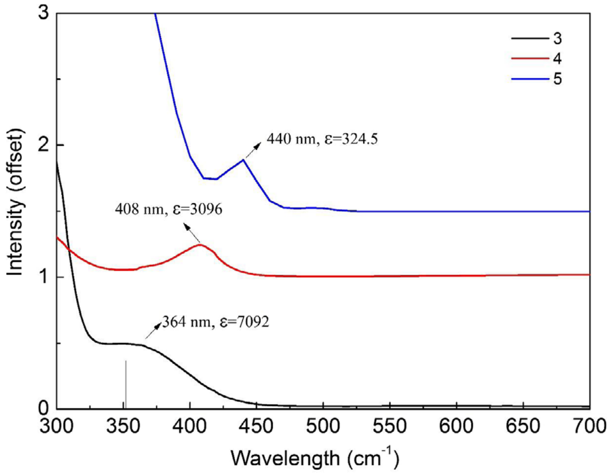

Figure 6. Experimental UV–vis spectra of **3**, **4** and **5** in DMSO (50 ppm).

that intra-ligand transitions of the organic ligands have lower intensities with similar results being obtained for Ir(I) complexes [25].

Assuming there is no intra-ligand π orbital, the allowed charge transfer transitions for square-planar complexes may be $^1A_{1g}$–$^1A_{2u}$ and $^1A_{1g}$–^1E_u [25, 26]. As should be anticipated, these transitions are from molecular orbitals mainly localized on the ligands to molecular orbitals mainly localized on metals. Both these transitions for **4** have moderate intensities and are located at around 408 nm ($\varepsilon \approx 3096\ M^{-1}\ cm^{-1}$) [26, 27]. Although the UV–vis spectrum of **4** showed a similar absorption to Ir(I) complexes, the UV–vis spectrum of **5** shows the peak at 440 nm ($\varepsilon \approx 325\ M^{-1}\ cm^{-1}$). It can be noted that the band at around 400 nm for **4** is shifted towards the high wavelength. This is mainly due to the fact that the influence of 4d electrons from the distortion and ligand-field strength are greater than that of the 5d electrons.

When the calculated and experimentally obtained bands are compared, it is seen that the experimentally obtained data of **3** are in agreement with the computational calculations. However, the experimentally obtained bands of **4** and **5** do not correspond to the calculated data and it should be pointed out that the calculations do not take into account *π* electrons. The experimental peaks do, however, have broad halos around the peaks, which includes the calculated data (Table 6).

Since Ir(I) has a d^8 electronic configuration, the highest level of filled d-orbitals is $b_{2g}(xy)$, such that the electronic ground state is $^1A_{1g}$ (as expected for all $^1A_{1g}$ ground-state electronic configurations, our complexes are diamagnetic also). It must be pointed out here that this labeling for the term symbols is named for pure square-planar complexes. Since our complexes are distorted square planar, one may use $^1A_1'$ instead of $^1A_{1g}$ which may indicate the distorted geometry. The energy level splitting of d orbitals in a square-planar environment is pictured in figure S3.

3. Experimental

3.1. Materials and methods

Unless stated otherwise, all manipulations were performed using standard Schlenk techniques under an argon or nitrogen atmosphere. Chemicals and solvents were purchased from Sigma Aldrich Co. (Dorset, UK) and used directly without further purifications. Solvents of analytical grade were freshly distilled using an MBraun SPS-800 solvent purification system. Mass spectra were recorded by ESI (electron spray ionization) method. ^{1}H NMR and ^{13}C NMR spectra were recorded using a Bruker Avance AMX 300 or 600. The chemical shifts are given as dimensionless δ values and are frequency-referenced relative to the peak for TMS for ^{1}H and ^{13}C. The NMR studies were carried out in high-quality 5 mm NMR tubes. Coupling constants (*J* values) are given in Hz. NMR multiplicities are abbreviated as follows: s = singlet, d = doublet, t = triplet, m = multiplet, bs = broad singlet.

3.1.1. General procedure for synthesis of N-aryl functionalized Re-NHC.HX

Compounds **1** and **2** were synthesized via reaction of 13-dibromopropane (**1**) or 14-diiodobutane (**2**) (10 mmol) with *N,N*′-bis(2-phenylbenzen)formamidine (10 mmol) in the presence of K_2CO_3 (5 mmol) in acetonitrile under aerobic conditions heated to reflux for 24 h (Figure 1). Solution was left to cool at room temperature and the solvent was removed *in vacuo*. Residue was solved in DCM (20 mL), filtered to separate all potassium salts and recrystallized via addition of diethylether to get white crystals.

3.1.2. *6-DiPh.HBr,* (1)

Yield: (3.42 g, 73%). mp. 256–258 °C (from dichloromethane). ^{1}H NMR (400 MHz, $CDCl_3$), *δ*/ppm: 1.17 [t, *J = 8 Hz*, 2H, $NCH_2\mathit{CH}_2CH_2$ N], 3.72 [t, *J = 8 Hz*, 4 H, $NC\mathit{H}_2CH_2C\mathit{H}_2$ N], 7.06–8.30 [m, 18H, $C_6H_4(C_6H_5)$-2], 7.77 [s, 1 H, NCHN]. ^{13}C NMR (100 MHz, $CDCl_3$), *δ*/ppm: 19.3, 47.5, 128.4, 128.6, 128.8, 129.2, 129.9, 130.1, 131.2, 137.3, 137.5, 154.7. $C_{28}H_{25}N_2Br$ (MW = 469.41): LCMS-MS (ESI): *m/z,* (%) 389.20 (100) $[M - Br]^+$.

3.1.3. *7-DiPh.HI,* (2)

Yield: (3.04 g, 75%). mp. 218–220 °C (from dichloromethane). ^{1}H NMR (600 MHz; DMSO-d_6), δ/ppm: 1.48 [br s, 4H, $NCH_2CH_2CH_2CH_2$ N], 3.81 [bs, 4H, $NCH_2CH_2CH_2CH_2$ N] 7.42–7.61 [m, 18H, $C_6H_4(C_6H_5)$-2], 8.56 [s, 1H, NCHN]. ^{13}C NMR (150 MHz, DMSO-d_6), *δ*/ppm: 23.5, 53.8, 127.1, 128.3, 128.9, 129.1, 129.7, 131.3, 137.4, 137.5, 141.5, 160.3. $C_{29}H_{27}N_2I$ (MW = 530.44), LCMS-MS (ESI): *m/z,* (%) 404.20 (100) $[M + H]^+$.

3.2. General procedure for synthesis of re-Ir-NHC and Re-Rh-NHC complexes

The general synthetic procedure for **3–5** is as follows: The desired Re-NHC.HBr (**1** or **2**) (1 mmol) was loaded into a flame-dried Schlenk and dried under high vacuum for 1 h before suspended in dry degassed THF (30 mL) and KHMDS *[au: The abbreviation should* *be given]* (1 mmol) added in glove box. The solution was stirred for 45 min at room temperature and transferred via an oven dried filter to a stirred THF solution of corresponding $[M(COD)Cl]_2$ (0.05 mmol) metal precursors. After the solution was stirred overnight at room temperature, solvents were removed under vacuum and residue yellow (in case of rhodium) or red solid (in case of iridium) was washed with cold hexane. For more purification of **3–5** were passed a short column of silica with DCM to get as microcrystalline solids.

3.2.1. *[IrCl(6-DiPh)(COD)]* (3)

Yield: (0.5 g, 75%). mp: 185–186 °C (from dichloromethane). UV–vis (DMSO), λ_{max}/nm: 440. ^1H NMR (300 MHz, $CDCl_3$), δ/ppm: 1.0–1.97 [m, 10H, $CHCH_2$ and $NCH_2CH_2CH_2$ N], 2.78 [t, $J = 2.4$ *Hz*, 2H, $CHCH_2$], 3.02 [m, 2H, NCH_2], 3.35 [m, 2H, NCH_2], 4.23 [t, $J = 2.4$ *Hz*, 2H, $CHCH_2$], 7.28–7.52 [m, 16H, $C_6H_4(C_6H_5)$-2], 8.90 [d, $J = 6.6$ *Hz*, 2H, $C_6H_4(C_6H_5)$-2]. ^{13}C NMR (75 MHz, $CDCl_3$), δ/ppm: 21.3, 28.3, 32.7, 49.5, 50.0, 80.1, 127.3, 127.6, 128.6, 128.8, 130.6, 133.5, 137.0, 140.1, 144.0, 205.9. Anal. Calcd for $C_{36}H_{36}N_2ClIr$ (%): C, 59.69; N, 3.87; H, 5.01. Found: C, 59.71; N, 4.01; H, 5.15.

3.2.2. *[RhCl(6-DiPh)(COD)]* (4)

Yield: 0.5 g (80%). mp: 168–169 °C (from dichloromethane). UV–vis (DMSO), λ_{max}/nm: 411. ^1H NMR (300 MHz, $CDCl_3$), δ/ppm: 1.33–1.89 [m, 10H, $CHCH_2$ and $NCH_2CH_2CH_2$ N], 2.90 [m, 2H, $CHCH_2$], 3.07 [m, 2H, NCH_2], 3.24 [m, 2H, NCH_2], 4.69 [m, 2H, $CHCH_2$], 7.28–7.65 [m, 16H, $C_6H_4(C_6H_5)$-2], 9.34 [d, $J = 9.0$ *Hz*, 2H, $C_6H_4(C_6H_5)$-2]. ^{13}C NMR (75 MHz, $CDCl_3$), δ/ppm: 21.1, 27.7, 31.8 49.4, 65.5, 65.8, 94.9, 95.0, 127.3, 127.7, 128.0, 128.6, 128.7, 130.8, 132.2, 140.1, 140.7, 212.3, 212.7. Anal. Calcd for $C_{36}H_{36}N_2ClRh$ (%): C, 68.09; N, 4.41; H, 5.71. Found: C, 68.13; N, 4.52; H, 5.82.

3.2.3. *[IrCl(7-DiPh)(COD)]* (5)

Yield: (0.29 g, 40%). mp: 220–222 °C (from dichloromethane). UV–vis (DMSO), λ_{max}/nm: 361, 430. ^1H NMR (300 MHz, $CDCl_3$), δ/ppm: 0.85–1.61 [m, 12H, $CHCH_2$ and $NCH_2CH_2CH_2CH_2$ N], 2.61 [m, 2H, $CHCH_2$], 3.28 [m, 2H, NCH_2], 3.69 [m, 2H, NCH_2], 4.14 [m, 2H, $CHCH_2$], 7.21–7.40 [m, 16H, $C_6H_4(C_6H_5)$-2], 8.77 [d, $J = 3.9$ *Hz*, 2H, $C_6H_4(C_6H_5)$-2]. ^{13}C NMR (75 MHz, $CDCl_3$), δ/ppm: 23.6, 28.1, 32.7, 49.3, 56.5, 81.0, 127.2, 127.3, 128.5, 128.9, 129.3, 130.5, 134.7, 137.2, 140.1, 144.5, 216.7. Anal. Calcd for $C_{37}H_{38}N_2ClIr$ (%): C, 60.19; N, 3.79; H, 5.19. Found: C, 60.32; N, 3.93; H, 5.36.

4. Conclusion

Synthesis and characterization of ring-expanded Ir and Rh-NHC complexes have been performed and the structure of complexes was determined by XRD, NMR and other spectroscopic techniques. DFT study of complexes on account heterocycle ring size and metal center diversity has been comparatively documented with experimental observations. According to the observations, it appears that the experimental and theoretical results obtained are highly compatible with each other. We calculated and compared the stability of the Ir and Rh re-NHC complexes by DFT calculations. The results represent that the seven-membered iridium complex, **5**, displays a higher chemical activity due to lower energy gap than the six-membered iridium, **3**, and rhodium complex, **4**.

Supplementary material

LCMS-MS spectra for **1** and **2**, NMR spectra for **1–5**, X-ray crystallographic data and refinement parameters and CIF for **3** (CCDC 1454752), **4** (CCDC 1511413) and **5** (CCDC 1511414) are supplied as supplementary file.

Acknowledgements

Authors give special thanks to Dr F. Işık who performed the Gaussian calculations in his lab.

Disclosure statement

No potential conflict of interest was reported by the authors.

Funding

This work was financially supported by the Scientific and Technological Research Council of Turkey (TÜBİTAK Project no 113Z285).

References

[1] (a) N. Marion, S. Diez-Gonzalez, S.P. Nolan. *Angew. Chem. Int. Ed.*, **46**, 2988 (2007); ; (b) D. Enders, O. Niemeier, A. Henseler. *Chem. Rev.*, **107**, 5606 (2007); (c) V. Nair, S. Bindu, V. Sreekumar. *Angew. Chem. Int. Ed.*, **43**, 5130 (2004).

[2] (a) A.J. Arduengo, R.L. Harlow, M. Kline. *J. Am. Chem. Soc.*, **113**, 361 (1991) ; (b) A.J. Arduengo. *Acc. Chem. Res.*, **32**, 913 (1999); For reviews see: F.E. Hahn, M.C. Jahnke. *Angew. Chem. Int. Ed.*, 47, 3122 (2008); W.A. Herrmann. *Angew. Chem. Int. Ed.*, **41**, 1290 (2002); (c) E.A.B. Kantchev, C.J. O'Brien, M.G. Organ. *Angew. Chem. Int. Ed.*, **46**, 2768 (2007); (d) J.J. Dunsford, D.S. Tromp, K.J. Cavell, C.J. Elsevier, B.M. Kariuki. *Dalton Trans.*, **42**, 7318 (2013); (e) D.G. Gusev. *Organometallics*, **28**, 6458 (2009); (f) R. Tonner, G. Frenking. *Organometallics*, **28**, 3901 (2009).

[3] (a) T. Droge, F. Glorius. *Angew. Chem. Int. Ed.*, **49**, 6940 (2010); (b) S.P. Nolan (Ed.). *N-Heterocyclic Carbenes in Synthesis*, 1st Edn, Wiley-VCH, Weinheim (2006); (c) F. Glorius (Ed.). *N-Heterocyclic Carbenes in Transition Metal Catalysis*, Springer, Berlin Heidelberg (2007); (d) S. Diez-Gonzalez. *N-Heterocyclic Carbenes From Laboratory Curiosities to Efficient Synthetic Tools*, Royal Society of Chemistry, Cambridge, UK (2011).

[4] (a) E.L. Kolychev, A.F. Asachenko, P.B. Dzhevakov, A.A. Bush, V.V. Shuntikov, V.N. Khrustalev, M.S. Nechaev. *Dalton Trans.*, **42**, 6859 (2013); (b) A.R. Leverett, A.I. McKay, M.L. Cole. *Dalton Trans.*, **44**, 498 (2015); (c) M. Iglesias, D.J. Beetstra, B. Kariuki, K.J. Cavell, A. Dervisi, I.A. Fallis. *Eur. J. Inorg. Chem.*, **13**, 1913 (2009); (d) J.J. Dunsford, K.J. Cavell, B.M. Kariuki. *Organometallics*, **31**, 4118 (2012).

[5] (a) W.Y. Lu, K.J. Cavell, J.S. Wixey, B.M. Kariuki. *Organometallics*, **30**, 5649 (2011); (b) J.J. Dunsford, K.J. Cavell. *Organometallics*, **33**, 2902 (2014); (c) C.C. Scarborough, I.A. Guzei, S.S. Stahl. *Dalton Trans.*, **13**, 2284 (2009); (d) C.C. Scarborough, A. Bergant, G.T. Sazama, I.A. Guzei, L.C. Spencer, S.S. Stahl. *Tetrahedron*, **65**, 5084 (2009); (e) C.C. Scarborough, M.J.W. Grady, I.A. Guzei, B.A. Gandhi, E.E. Bunel, S.S. Stahl. *Angew. Chem. Int. Ed.*, **44**, 5269 (2005).

[6] (a) R. Singh, M.S. Viciu, N. Kramareva, O. Navarro, S.P. Nolan. *Org. Lett.*, **7**, 1829 (2005); (b) N. Marion, O. Navarro, J.G. Mei, E.D. Stevens, N.M. Scott, S.P. Nolan. *J. Am. Chem. Soc.*, **128**, 4101 (2006); (c) A. Chartoire, M. Lesieur, L. Falivene, A.M.Z. Slawin, L. Cavallo, C.S.J. Cazin, S.P. Nolan. *Chem. Eur. J.*, **18**, 4517 (2012).

[7] M. Iglesias, D.J. Beetstra, J.C. Knight, L.L. Ooi, A. Stasch, S. Coles, L. Male, M.B. Hursthouse, K.J. Cavell, A. Dervisi, I.A. Fallis. *Organometallics*, **27**, 3279 (2008).

[8] (a) G. Altenhoff, R. Goddard, C.W. Lehmann, F. Glorius. *Angew. Chem. Int. Ed.*, **42**, 3690 (2003); (b) S. Wurtz, F. Glorius. *Acc. Chem. Res.*, **41**, 1523 (2008).

[9] (a) F. Godoy, C. Segarra, M. Poyatos, E. Peris. *Organometallics*, **30**, 684 (2011); (b) C.S. Zhou, J.Y. Wang, L.Y. Li, R.H. Wang, M.C. Hong. *Green Chem.*, **13**, 2100 (2011); (c) T. Tu, X.K. Feng, Z.X. Wang, X.Y. Liu. *Dalton Trans.*, **39**, 10598 (2010).

[10] N. Marion, O. Navarro, J. Mei, E. Stevens, N. Scott, S. Nolan. *J. Am. Chem. Soc.*, **128**, 4101 (2006).

[11] W.A. Herrmann, S.K. Schneider, K. Öfele, M. Sakamoto, E. Herdtweck. *J. Organomet. Chem.*, **689**, 2441 (2004).

[12] M. Mayr, K. Wurst, K.H. Ongania, M.R. Buchmeiser. *Chem. Eur. J.*, **10**, 1256 (2004).

[13] N. Imlinger, M. Mayr, D.R. Wang, K. Wurst, M.R. Buchmeiser. *Adv. Synth. Catal.*, **346**, 1836 (2004).

[14] D.T. Houghton, N.W. Gydesen, N. Arulsamy, and M.P. Mehn. *Inorg.Chem.*, **49**, 879 (2010).

[15] G.M. Sheldrick. *Acta Crystallogr.*, **A64**, 112 (2008).

[16] L.J. Farrugia. *J. Appl. Crystallogr.*, **30**, 565 (1997).

[17] S. Yasar, K.J. Cavell, B.D. Ward, B. Kariuki. *Appl. Organomet. Chem.*, **25**, 374 (2011).

[18] J.-F. Sun, F. Chen, B.A. Dougan, H.-J. Xu, Y. Cheng, Y.-Z. Li, X.-T. Chen, Z.-L. Xue. *J. Organomet. Chem.*, **694**, 2096 (2009).

[19] D. Cremer, J.A. Pople. *J. Am. Chem. Soc.*, **97**, 1354 (1975).

[20] Frisch M.J., Trucks G.W., Schlegel H.B., Scuseria G.E., Robb M.A., *Gaussian 09, Revision D.01*, Gaussian, Inc., Wallingford, CT (2009).

[21] R. Dennington, T. Keith, J. Millam. *Gauss View, Version 5.*, Semichem Inc., Shawnee Mission, KS (2009).

[22] P. Politzer, D.G. Truhlar. *Chemical Applications of Atomic and Molecular Electrostatic Potentials*, Springer Science, New York, NY (1981).

[23] S. Bahçeli, H. Gökçe. *Can. Chem. Trans.*, **2**, 175 (2014).

[24] (a) L.R. Collins, T.M. Rookes, M.F. Mahon, I.M. Riddlestone, M.K. Whittlesey. *Organometallics*, **33**, 5882 (2014); (b) J.J. Dunsford, K.J. Cavell. *Dalton Trans.*, **40**, 9131 (2011).

[25] A.K. Brisdon. *UV–visible Spectroscopy.*, Inorganic Spectroscopic Methods, Oxford, UP (1998).

[26] M.J. Alcón, M. Iglesias, F. Sánchez, I. Viani. *J. Organomet. Chem.*, **634**, 25 (2001).

[27] N. Kanematsu, M. Ebihara, T. Kawamura. *Inorg. Chim. Acta*, **292**, 244 (1999).